

SageAttention2: Efficient Attention with Thorough Outlier Smoothing and Per-thread INT4 Quantization

Jintao Zhang^{*1} Haofeng Huang^{*1} Pengle Zhang¹ Jia Wei¹ Jun Zhu¹ Jianfei Chen¹

Abstract

Although quantization for linear layers has been widely used, its application to accelerate the attention process remains limited. To further enhance the efficiency of attention computation compared to SageAttention while maintaining precision, we propose SageAttention2, which utilizes significantly faster 4-bit matrix multiplication (Matmul) alongside additional precision-enhancing techniques. First, we propose to quantize matrices (Q, K) to INT4 in a hardware-friendly thread-level granularity and quantize matrices (\tilde{P}, V) to FP8. Second, we propose a method to smooth Q , enhancing the accuracy of INT4 QK^\top . Third, we propose a two-level accumulation strategy for $\tilde{P}V$ to enhance the accuracy of FP8 $\tilde{P}V$. The operations per second (OPS) of SageAttention2 surpass FlashAttention2 and xformers by about **3x** and **4.5x** on RTX4090, respectively. Moreover, SageAttention2 matches the speed of FlashAttention3(fp8) on the Hopper GPUs, while delivering much higher accuracy. Comprehensive experiments confirm that our approach incurs negligible end-to-end metrics loss across diverse models—including those for language, image, and video generation. [The code is available at https://github.com/thu-ml/SageAttention](https://github.com/thu-ml/SageAttention)

1. Introduction

Due to the quadratic time complexity of attention, its efficient implementation becomes crucial as sequence lengths increase in real-world applications (Jiang et al., 2024). Several strategies have been developed to mitigate computational demands of attention—such as (1) *Linear attention* methods (Wang et al., 2020; Choromanski et al., 2021; Yu et al., 2022; Katharopoulos et al., 2020) that reduce complexity to $O(N)$ and (2) *Sparse attention* methods (Liu et al.,

2021; Chu et al., 2021; Li et al., 2022; Xiao et al., 2024b;a; Chen et al., 2024; Jiang et al., 2024; Venkataramanan et al., 2024; Gao et al., 2024; Fu et al., 2024) that selectively process parts of the context—these methods are only suitable for a limited range of models and tasks. The widely used attention methods optimize attention by exploiting hardware capacities, such as FlashAttention (Dao et al., 2022), FlashAttention2 (Dao, 2024), FlashAttention3 (Shah et al., 2024), xformers (Lefaudeux et al., 2022), and SageAttention (Zhang et al., 2025). These works do not omit computations across the entire sequence and achieve impressive speed and accuracy performance across various tasks.

Motivation. For the two matrix multiplication (Matmul) operations in attention: QK^\top and $\tilde{P}V$, SageAttention accelerates them by quantizing the QK^\top to INT8 and uses FP16 Matmul with FP16 accumulators for $\tilde{P}V$. Moreover, to keep the accuracy of attention, SageAttention proposes smoothing K by eliminating its channel-wise outliers. SageAttention achieves $2 \times$ speedup than FlashAttention2 and is the first quantized attention that incurs negligible end-to-end metrics loss across language, image, and video generation models. However, SageAttention has two weaknesses. **(W1)** INT8 Matmul achieves only half the speed of INT4. **(W2)** FP16 Matmul with FP16 accumulators provides a speedup only on RTX 4090 and RTX 3090 GPUs. To leverage the faster INT4 tensor cores for QK^\top and using a method that can accelerate $\tilde{P}V$ on a broader range of GPUs, we propose to quantize Q, K to INT4 and \tilde{P}, V to FP8.

Challenges. Quantizing Q, K to INT4 and \tilde{P}, V to FP8 presents significant challenges. For example, when only per-tensor quantizing Q, K to INT4, the text-to-video model CogvideoX will generate a completely blurry video, and Llama3 only achieves a random-guessing-level accuracy of 25% on MMLU. After investigating deeply, we identified three primary challenges: **(C1)** The numerical range of INT4 is quite limited compared to FP16 or INT8, leading to significant quantization errors when Q and K have some abnormal values. **(C2)** We discover that the FP32 accumulator designed for FP8 matrix multiplication in the tensor core (`mma.f32.f8.f8.f32`) is actually FP22, specifically with 1 sign bit, 8 exponent bits, and 13 mantissa bits. This will lead to an accuracy loss of $\tilde{P}V$.

^{*}Equal contribution ¹Department of Computer Science and Technology, Tsinghua University. Correspondence to: Jianfei Chen <jianfeic@tsinghua.edu.cn>. *Preprint.*

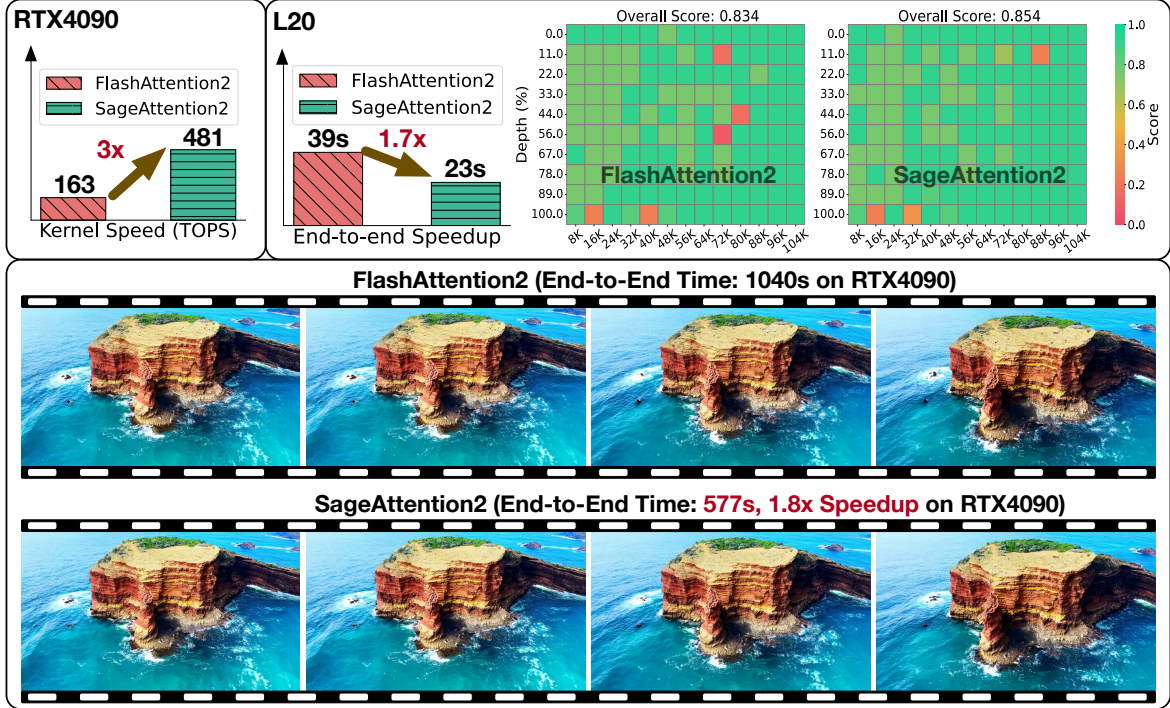


Figure 1. The upper left figure shows the kernel speedup on RTX4090 GPU. The upper right figure shows the end-to-end inference speedup of generating the first token and performance metrics for the Needle-in-a-Haystack task (Kamradt, 2023) with a sequence length of 100K on Llama3.1 on L20 GPU. The figure below shows two videos generated by CogVideoX (1.5-5B) using FlashAttention2 and SageAttention2 on RTX4090, showing that SageAttention2 accelerates generation by 1.8x with no video quality loss.

Our approach. To address (C1), we first discover that the per-block quantization of Q, K in SageAttention does not achieve sufficient accuracy for INT4 quantization. Simultaneously, to avoid the extra latency caused by per-token dequantization, where each GPU thread corresponds to multiple quantization scales, we propose an adequately precise quantization method that incurs no additional dequantization overhead. Specifically, we introduce a per-thread quantization approach based on the mapping between the GPU threads and memory layout of matrices as dictated by the PTX `mma` instructions. This method groups tokens corresponding to the same thread for quantization and dequantization, ensuring that each thread is associated with a single quantization scale. This approach achieves much better accuracy performance than per-block quantization with no additional dequantization overhead. Second, for the significant channel-wise outliers in matrices Q and K , we adopt smoothing K in SageAttention and further propose an effective method to remove these outliers in Q . Specifically, we propose subtracting the average value of the channel dimension of Q , referred to as \vec{Q}_m . Then, we add $\vec{Q}_m K$ after the QK^T Matmul to ensure the correctness of the attention computation. To address (C2), the accuracy loss from the 22-bit accumulator for FP8 Matmul of $\tilde{P}V$, we propose a two-level accumulation strategy that uses an FP32 buffer to accumulate the values from the 22-bit accumulator after each block Matmul of $\tilde{P}V$. This method confines the errors

to the block range. Additionally, we design an optional technique to enhance the accuracy of the 22-bit accumulator. Specifically, we could smooth V by subtracting the average value of its channel dimension and adding the subtracted item to the attention output to maintain the correctness.

Performance. Importantly, we offer a high-performance implementation of SageAttention2 on RTX4090 and L20 GPUs. This implementation achieves a peak performance of **481 TOPS** on the RTX4090, outperforming FlashAttention2 and xformers by approximately 3x and 4.5x, respectively. Note that FlashAttention3 is tailored to and can only be used with the Nvidia Hopper architecture. Moreover, SageAttention2 matches the speed of FlashAttention3(fp8) on the Hopper GPUs, while delivering much better accuracy. For example, on CogVideoX-1.5 (Yang et al., 2025), Mochi (Team, 2024) and HunyuanVideo (Kong et al., 2024), our method does not compromise end-to-end accuracy, whereas videos generated using FlashAttention3(fp8) often suffer noticeable degradation, as visualized in Fig. 8. We extensively evaluate the end-to-end metrics of state-of-the-art text, image, and video generation models using SageAttention2. SageAttention2 can accelerate models in a plug-and-play way with negligible loss in end-to-end metrics.

2. Preliminary

2.1. FlashAttention

The attention computation can be formulated as: $S = QK^\top/\sqrt{d}$, $P = \sigma(S)$, $O = PV$, where $\sigma(S)_{ij} = \exp(S_{ij})/\sum_k \exp(S_{ik})$. The matrices Q , K , and V each has dimensionality $N \times d$, and S , P are $N \times N$. d is typically small, e.g., 64 or 128, and N can be thousands or millions. The time complexity of attention is $O(N^2)$, primarily due to two matrix multiplications (QK^\top and PV), both with complexities of $O(N^2d)$. FlashAttention (Dao, 2024) is a GPU-friendly attention implementation, which tiles Q , K , and V from the token dimension into blocks $\{Q_i\}_{i=1}^{n_q}$, $\{K_i\}_{i=1}^{n_k}$, $\{V_i\}_{i=1}^{n_v}$ with block sizes of b_q , b_k , b_v tokens, respectively, where n_q, n_k, n_v are the number of tiles, and $b_k = b_v$. FlashAttention computes the output matrix O in parallel in tiles. Each streaming multiprocessor (SM) computes a block O_i (corresponds to a Q_i) by iteratively loads K_j, V_j for each j , and update the output with online softmax (Milakov & Gimelshein, 2018):

$$\begin{aligned} S_{ij} &= Q_i K_j^\top / \sqrt{d}, \quad (m_{ij}, \tilde{P}_{ij}) = \tilde{\sigma}(m_{i,j-1}, S_{ij}), \quad (1) \\ l_{ij} &= \exp(m_{i,j-1} - m_{ij}) l_{i,j-1} + \text{rowsum}(\tilde{P}_{ij}), \\ O_{ij} &= \text{diag}(\exp(m_{i,j-1} - m_{ij})) O_{i,j-1} + \tilde{P}_{ij} V_j, \end{aligned}$$

where m_{ij} and l_{ij} are b_q -dimensional vectors, initialized with $-\infty$ and 0 respectively. $\tilde{\sigma}(\cdot)$ is an online softmax operator: $m_{ij} = \max\{m_{i,j-1}, \text{rowmax}(S_{ij})\}$, $\tilde{P}_{ij} = \exp(S_{ij} - m_{ij})$. Finally, the output is computed as $O_i = \text{diag}(l_{i,n_q})^{-1} O_{i,n_q}$.

2.2. Quantization

A matrix multiplication $C = AB$ can be accelerated with quantization as:

$$(\delta_A, \hat{A}) = \psi(A), \quad (\delta_B, \hat{B}) = \psi(B), \quad C = \psi_{\delta_A \delta_B}^{-1}(\hat{A} \hat{B})$$

ψ is a *quantizer* which converts a high-precision (e.g., FP32 or FP16) matrix A to a low-precision format \hat{A} (e.g., INT4 or FP8) with a *scale* δ_A , and ψ^{-1} is a *dequantizer* to convert back to high-precision. We should have $\psi_{\delta_A}^{-1}(\hat{A}) \approx A$. The actual matrix multiplication $\hat{A} \hat{B}$ is carried out with low precision. In modern GPUs, low-precision matrix multiplication is usually multiple times faster than higher-precision ones. Quantizers differ in *numerical format* and *granularity*, e.g., how many elements (“quantization group”) share a common scale factor. For example, an *INT4, per-tensor quantizer* first computes the scale as the maximum absolute value of the entire tensor, scales the elements to the maximum representable range of INT4 $[-7, +7]$, and then casts to INT4 with rounding: $\hat{A} = \lceil A/\delta_A \rceil$, $\delta_A = \max(|A|)/7$. The dequantization process is an element-wise scaling. For example, for per-tensor dequantization, $\psi_{\delta_A \delta_B}^{-1}(\hat{A} \hat{B}) = \hat{A} \hat{B} \times \delta_A \delta_B$.

Table 1. Speedup compared to matrix multiplication in FP16 with an FP32 accumulator.

GPU	MM Input	MM Accumulator	Speedup
RTX4090	FP16	FP16	2x
	FP8	FP32	2x
L40, L20 H100	FP16	FP16	1x
	FP8	FP32	2x

2.3. SageAttention

Based on the block tiling in FlashAttention (Dao et al., 2022), SageAttention (Zhang et al., 2025) quantizes Q, K to INT8 in a per-block granularity, i.e., each Q_i, K_i has a separate scalar scale: $\delta_{Q_i} = \max(|Q_i|)/127$, $\delta_{K_j} = \max(|K_j|)/127$. In this way, the product S_{ij} in Eq. (1) can be approximated as $S_{ij} \approx \hat{Q}_i \hat{K}_j^\top \times (\delta_{Q_i} \delta_{K_j} / \sqrt{d})$. To maintain the accuracy, SageAttention proposes a preprocessing technique to by subtracting the token-wise mean from K . Additionally, SageAttention keeps \tilde{P}_{ij} and V_j in FP16, but utilizes an FP16 accumulator (rather than FP32) for computing the product $\tilde{P}_{ij} V_j$. Reducing the accumulator precision can accelerate the matrix multiplication (MM) on RTX4090 GPU. However, other GPUs, such as L20, L40, or H100, do not exhibit this behavior, as shown in Table 1.

3. SageAttention2

In this section, we introduce SageAttention2, an efficient and accurate quantized attention. The workflow of SageAttention2 is shown in Fig. 2. We quantize Q, K to INT4 and \tilde{P}, V to FP8 to maximize the efficiency and propose several techniques, including QK -smoothing, per-thread quantization, and two-level accumulation to preserve the accuracy, which we shall discuss in subsequent subsections.

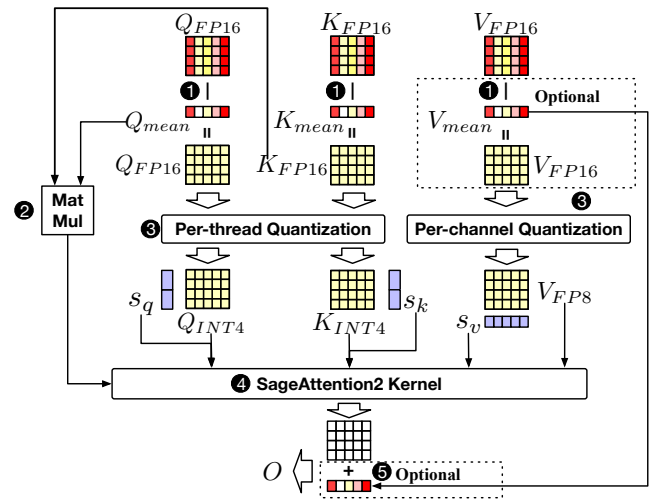


Figure 2. Workflow of SageAttention2. ① Smooth Q, K, V . ② A GEMV to obtain ΔS . ③ Per-thread quantize Q, K and per-channel quantize V . ④ Perform the SageAttention2 kernel. ⑤ Correct the output.

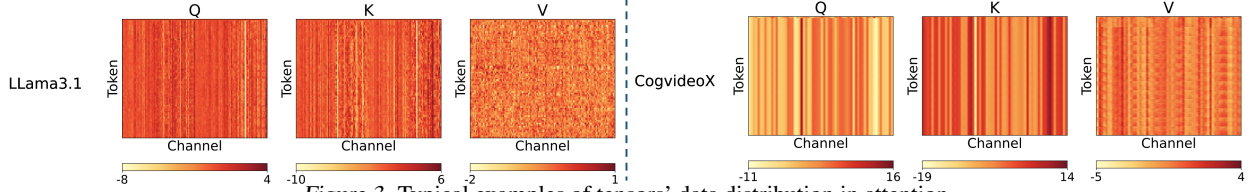


Figure 3. Typical examples of tensors' data distribution in attention.

3.1. Smooth Q

First, we discuss how to accurately compute QK^\top with INT4. The numerical range of INT4 is notably restrictive. This affects quantization due to the presence of *outliers* (Lin et al., 2024). Given the INT4 range $[-7, +7]$, any element will be quantized to zero if it is more than 14 times (0.5 vs 7) smaller than the largest element in the group. Since outliers are much larger than other elements, it is quite likely that most non-outlier elements are quantized to zero, resulting in significant accuracy degradation. Therefore, to keep the quantization accurate, we need to keep the largest element small, making the magnitude of elements as uniform as possible. Such technique is called *smoothing*.

Here, we propose a smoothing technique inspired by SageAttention (Zhang et al., 2025). SageAttention observed that Q, K for all tokens are actually highly similar, with only small variations between different tokens (see Fig. 3). We propose to smooth K as SageAttention does and further smooth Q by subtracting a common mean of each block:

$$\gamma(Q_i) = Q_i - \bar{q}_i, \quad \gamma(K_j) = K_j - \bar{k}, \quad (2)$$

where $\bar{q}_i = \text{mean}(Q_i)$, $\bar{k} = \text{mean}(K)$ are $1 \times D$ vectors, the mean is conducted along the token axis, and \bar{q}_i, \bar{k} are broadcasted to tokens in a block and a tensor for subtraction, respectively.

With the decomposition, we have $S_{ij} = Q_i K_j^\top = (\bar{q}_i + \gamma(Q_i))(\bar{k} + \gamma(K_j))^\top = \bar{q}_i \bar{k}^\top + \bar{q}_i \gamma(K_j)^\top + \gamma(Q_i) \bar{k}^\top + \gamma(Q_i) \gamma(K_j)^\top = \bar{q}_i \gamma(K_j)^\top + \gamma(Q_i) \bar{k}^\top + \Delta S_{ij} + b$. Here, $\Delta S_{ij} = \bar{q}_i \gamma(K_j)^\top$ is an $1 \times N$ vector, and $b = \bar{q}_i \bar{k}^\top + \gamma(Q_i) \bar{k}^\top$ is an $N \times 1$ vector. We do not need to compute b since adding a common bias to an entire row of S does not affect the result after softmax. Therefore, we can accelerate $Q_i K_j^\top$ with INT4 by the following two stages:

(1) *preprocessing*: smooth Q, K according to Eq. (2), apply quantization $(\delta_{Q_i}, \hat{Q}_i) = \psi_Q(\gamma(Q_i))$, $(\delta_{K_j}, \hat{K}_j) = \psi_K(\gamma(K_j))$, and compute $\Delta S_{ij} = \bar{q}_i \gamma(K_j)^\top$. The smoothing, quantization, and the GEMV (general matrix-vector multiplication) for computing ΔS can be fused into a single kernel, which scans the off-chip Q and K only once.

(2) *attention*: execute the low-precision GEMM, dequantize, and add back the vector ΔS : $S_{ij} = \psi_{\delta_{Q_i} \delta_{K_j}}^{-1}(\hat{Q}_i \hat{K}_j^\top) + \Delta S_{ij}$. These operations are all done on chip, and the dequantization and vector addition only adds a marginal overhead compared to the expensive mma operation for MM.

Importantly, $\gamma(Q_i), \gamma(K_j)$ are quantized rather than Q_i, K_j .

Since the smoothed matrices are much smaller in magnitude and contain less outliers, the quantization accuracy can be significantly improved.

Remark. Classical techniques to improve the activation-weight MM, such as per-channel quantization, or SmoothQuant (Xiao et al., 2023) are not applicable here for the query-key MM in attention. Per-channel quantization is impracticable for Q, K because quantization must be conducted along the outer axis (token dimension) of QK^\top (Xiao et al., 2023). On the other hand, both Q and K have significant outliers, so trading the quantization accuracy between them with SmoothQuant cannot work effectively, as shown in Sec. 4.1. Here, we utilize the unique token-similarity pattern in attention to derive an accurate dedicated quantization method for Q and K . The previous work SageAttention only smooths K , so it is less accurate than our method.

Empirical results. Fig. 19 in Appendix A.7 shows an example from CogvideoX of the distribution of \hat{Q} with and without smoothing Q . We can find that with smoothing Q , the range of INT4 is utilized more uniformly and fully. Table 5 presents end-to-end metrics for different quantization methods with and without *smoothing* $Q+K$ on Llama3.1 (Dubey et al., 2024) and CogvideoX (2b) (Yang et al., 2025). The results demonstrate that *smoothing* $Q+K$ offers significant accuracy benefits. Also, Table 4 and 17 show that the order of effectiveness is *smoothing* $Q+K > \text{smoothing } Q > \text{smoothing } K > \text{other baselines}$.

3.2. INT4 Per-thread Quantization

Orthogonal to smoothing, we can mitigate the problem of outliers by refining the quantization granularity so the number of affected elements by outliers becomes smaller. Although per-token offers a detailed level of granularity, it results in significant overhead during dequantization. Specifically, each GPU thread in per-token quantization must handle multiple quantization scales, leading to a high latency of the dot product of the quantization scale vectors δ_Q and δ_K . SageAttention uses per-block quantization, where each block Q_i (b_q tokens) and K_i (b_k tokens) have a single quantization scale. Such a quantization strategy could achieve an accuracy performance close to per-token quantization and avoid the high dequantization overhead. However, quantizing Q and K to INT4 demands a finer quantization granularity. To address this, we propose *per-*

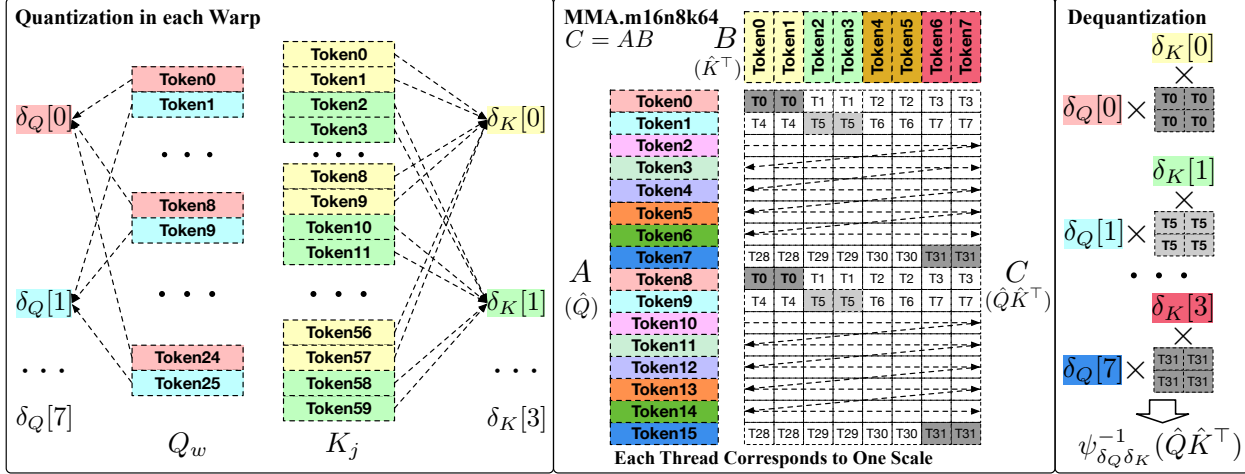


Figure 4. An example of per-thread quantization. The left figure shows the correspondence between the quantization scales and the tokens in each GPU warp. The right figure shows the correspondence between quantization tokens and GPU threads in a `MMA.m16n8k64` instruction, showing that each GPU thread only corresponds to one quantization scale in δ_Q and δ_K in dequantization.

thread quantization, a more precise and granular approach than the *per-block quantizer*, also without the additional overhead of vectors dot product between δ_Q and δ_K .

Specifically, each block of Q , i.e., Q_i , in SageAttention will be split into c_w segments and processed by c_w GPU warps in a GPU streaming processor (SM). We call each segment of Q_i as Q_w , and $k_w = K_j$ since K_j is shared among warps. Then, each warp containing 32 threads uses the `mma.m16n8k64` PTX instruction (NVIDIA) for the $Q_w K_j^\top$. According to the layout requirement of this instruction, we find that $Q_w[8k+i]$ could share one quantization scale, and $K_j[8k+2i]$ and $K_j[8k+2i+1]$ could share one quantization scale. Such a quantization method is more fine-grained and with no additional overhead. This is because it assigns different GPU threads to distinct quantization groups based on the MMA instruction layout, with each thread performing dequantization only using a single quantization scale value. We show an example of per-thread quantization in Fig. 4. The detailed formulation is shown in Equation 3 and Fig. 17 (Please see Appendix A.5 for more detail).

Empirical results. As shown in Table 6 and Table 15, we compare the average and the worst accuracy of INT4 quantization at per-token, per-thread, per-block, and per-tensor granularity using real Q, K, V across all layers of CogvideoX. Results indicate the accuracy of per-thread quantization is very close to per-token and outperforms a lot more than others.

3.3. FP8 quantization for $\tilde{P}V$

We now turn to the MM $\tilde{P}V$, where $\tilde{P}_{ij} = \exp(S_{ij} - m_{ij})$ is the unnormalized quantity according to Eq. (1). The distribution of \tilde{P} is unique and differs from other activations. First, we note that $S_{ij} - m_{ij} \leq 0$, so $P_{ij} \in [0, 1]$ (\leq and

\in apply element-wisely). We find that \tilde{P} often consists of many small elements, but their sum is non-negligible (e.g., 5000 elements around 10^{-4}). In this case, we must represent small elements accurately. INT quantization is unsuitable for this proposal since it puts the quantization points evenly within the numerical range. SageAttention (Zhang et al., 2025) choose to retain \tilde{P} and V in FP16, and accelerate the MM by decreasing the accumulator precision. However, this strategy is only effective on very few GPUs.

We propose to quantize \tilde{P}, V to FP8 with 4 exponent bits and 3 mantissa bits (E4M3). The numerical range of E4M3 is $[-448, +448]$. We quantize P with a static scale: $\delta_P = \frac{1}{448}$ since the original P elements is already in $[0, 1]$. We quantize V per-channel to address the channel-wise outliers shown in Fig. 3. Empirical results in Table 7 and Table 16 show the average and the worst accuracy of different data types used for \tilde{P}, V across all layers of CogvideoX. The accumulator is always 32-bit. We can see that the accuracy of E4M3 is very close to that of FP16 and superior to E5M2 and INT8. Most modern GPUs have tensor cores that support FP8 Matmul operations, which are twice as fast as those using FP16.

3.4. FP32 MMA Buffer for FP22 Accumulator

While FP8 quantization for $\tilde{P}V$ above is theoretically accurate in simulation, we observe that the actual CUDA implementation suffers a consistent accuracy degradation. After narrowing down the problem, we find that the accumulator for the `mma(f32f8f8f32)` instruction on the Ada and Hopper architecture is actually FP22, specifically with 1 sign bit, 8 exponent bits, and 13 mantissa bits. Specifically, for `mma(f32f8f8f32)` instruction $C = AB + D$, where A, B are FP8 matrices and C, D are FP32 matrices, we initialize the A, B to zero and vary D to test the data type of the accumulator. When D is initialized with 1 sign bit, 8

Algorithm 1 Implementation of SageAttention2.

Input: Matrices $Q(\text{FP16}), K(\text{FP16}), V(\text{FP16}) \in \mathbb{R}^{N \times d}$, block size b_q, b_{kv} , warp count c_w .

Preprocessing: $\bar{K} = K - \text{mean}(K)$, $(\delta_V, \tilde{V}) = \psi_V(V)$. //per-channel.

Divide Q to $T_m = N/b_q$ blocks $\{Q_i\}$; divide K , and V to $T_n = N/b_{kv}$ blocks $\{K_i\}, \{V_i\}$;

for $i = 1$ **to** T_m **do**

$\bar{q}_i = \text{mean}(Q_i)$, $(\delta_Q, \hat{Q}_i) = \psi_Q(Q_i - \bar{q}_i)$ //per-thread ;

for j in $[1, T_n]$ **do**

$(\delta_K, \hat{K}_j) = \psi_K(K_j)$ //per-thread, $w = \text{range}(c_w), st = w * c_w$;

$S_{ij}[st : st + c_w] = \psi_{\delta_Q \delta_K}^{-1}(\text{Matmul}(\hat{Q}_i[st : st + c_w], \hat{K}_j^\top)) + \text{GEMV}(\bar{q}_i, K_j^\top)$; // Paralleled by c_w warps. The $\psi_{\delta_Q \delta_K}^{-1}$ is illustrated in Fig. 4.

$m_{ij} = \max(m_{i,j-1}, \text{rowmax}(S_{ij}))$, $\tilde{P}_{ij} = \exp(S_{ij} - m_{ij})$, $l_{ij} = e^{m_{i,j-1} - m_{ij}} + \text{rowsum}(\tilde{P}_{ij})$;

$O_{ij}(\text{FP22}) = \text{Matmul}((\tilde{P}_{ij} * 448).\text{to}(\text{FP8.e4m3}), V_j)$;

$O_{ij}(\text{FP32}) = \text{diag}(e^{m_{i,j-1} - m_{ij}})^{-1} O_{i,j-1}(\text{FP32}) + O_{ij}(\text{FP22})$;

end for

Load δ_V into an SM ; $O_i = \text{diag}(l_{i,T_n})^{-1} O_{i,T_n}(\text{FP32}) / 448 * \delta_V$; Write O_i ;

end for

return $O = \{O_i\}$

exponent bits, and 13 mantissa bits, the value of C matches the result of the high-precision `mma(f16f16f32)` instruction. However, when D is initialized with more than 13 mantissa bits, the error of C corresponds to the difference between the results of `mma(f32f16f16f32)` and `mma(f32f8f8f32)`. Consequently, the matrix multiplication of $\tilde{P}V$, quantized to FP8, incurs a certain degree of accuracy loss compared to using an FP32 accumulator.

To mitigate this accuracy loss, we adopt a two-level accumulation strategy, which uses an FP32 buffer to accumulate the values of $\tilde{P}_{ij}V_j$ in FP22. Specifically, we rewrite Eq. (1) as $R_{ij} = \tilde{P}_{ij}V_j$, $O_{ij} = \text{diag}(\exp(m_{i,j-1} - m_{ij})) O_{i,j-1} + R_{ij}$. Here, two sets of accumulators R_{ij} and O_{ij} are maintained in the register. R_{ij} is computed with the `mma(f32f8f8f32)` instruction, providing 22 effective bits, which is sufficient since we only accumulate over a small number of b_k tokens (e.g., $b_k = 64$). Then, R_{ij} is accumulated to O_{ij} in the high FP32 precision.

Remark. The two-level accumulation strategy is also implemented in Cutlass (NVIDIA, 2023) and DeepSeekv3 (DeepSeek-AI et al., 2024) for computing activation-weight products in linear layers. To the best of our knowledge, we are the first to discover and investigate the effect of the FP22 accumulator and implement the two-level accumulation for *attention*.

Optional smooth V technique. We also figure out another way to mitigate the accuracy loss due to the FP22 accumulator when V possesses channel-wise biases: $\vec{V}_m = \text{mean}(V, \text{axis} = 0)$, $V = V - \vec{V}_m$. Additionally, to maintain the correctness of the attention computation, it is only necessary to add \vec{V}_m to the final calculation of O : $O = O + \vec{V}_m$. This is because the sum of each row of the \tilde{P} matrix equals 1, so $\tilde{P}\vec{V}_m = \vec{V}_m$.

Remark. For details on smoothing V, see Appendix A.3.

This technique is optional and not employed in our main experiments, as it provides significant benefits only when V exhibits channel-wise bias, which are absent in some models, such as Llama3.1 (see Fig. 3).

4. Experiment

Main result. SageAttention2 is faster than FlashAttention2 and xformers by approximately **3x** and **4.5x**, respectively. Moreover, SageAttention2 matches the speed of FlashAttention3(fp8) on the Hopper GPUs and is much more accurate than FlashAttention3(fp8). Our approach maintains end-to-end metrics across language, image, and video generation models.

4.1. Setup

Models. We validate the effectiveness of SageAttention2 across a diverse set of representative models from language, image, and video generation. Specifically, we conduct experiments on ten models: Llama2 (7B) (Touvron et al., 2023), Llama3.1 (8B) (Dubey et al., 2024), and GLM4 (9B) (GLM et al., 2024) for text2text, CogvideoX (2B), CogvideoX (1.5-5B) (Yang et al., 2025), HunyuanVideo (Kong et al., 2024), and Mochi (Team, 2024) for text2video, Flux (schnell) (Black Forest Labs, 2023) and Stable-Diffusion3.5 (turbo) (Stability AI, 2023) for text2image, and TIMM (Wightman, 2019) for image classification.

Datasets and metrics. For Details about the datasets and metrics we used, please refer to Appendix. A.6.

Table 3. Two kernel implementations of SageAttention2.

Kernel	$\psi_Q(Q), \psi_K(K)$	$\psi_P(\tilde{P}), \psi_V(V)$
SageAttn2-4b	INT4 per-thread	FP8 per-block and per-channel
SageAttn2-8b	INT8 per-thread	FP8 per-block and per-channel

Implementatation. We implement two attention kernels as

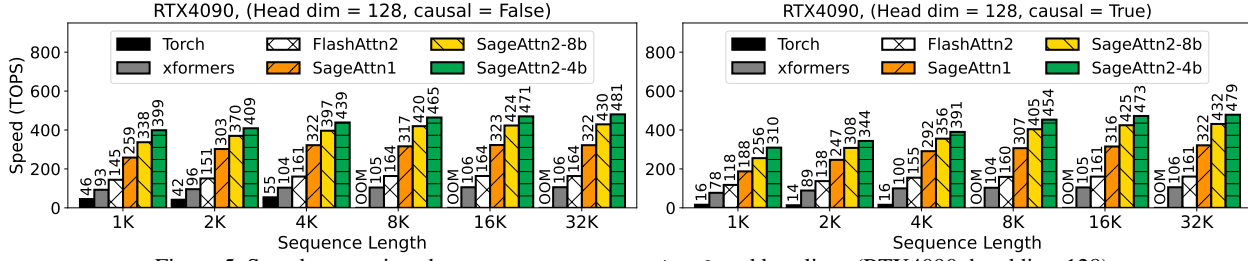


Figure 5. Speed comparison between SageAttention2 and baselines (RTX4090, headdim=128).

 Table 2. End-to-end metrics across text, image, and video generation models. **X** indicates an inability to generate results for evaluation.

Model	Attention	WikiText (Ppl.) ↓	Lambda (Acc.) ↑	MMLU (Acc.) ↑	Longbench ↑	
Llama3.1	Full-Precision	6.013	0.815	0.635	49.40	
	HadmdAttn	7.872	0.762	0.500	44.07	
	SmoothAttn	7.180	0.783	0.541	44.69	
	SageAttention	6.017	0.812	0.634	49.55	
	SageAttn2-4b	6.256	0.798	0.607	48.79	
	SageAttn2-8b	6.019	0.811	0.634	49.59	
GLM4	Full-Precision	7.241	0.432	0.743	49.78	
	HadmdAttn	7.989	0.435	0.669	45.97	
	SmoothAttn	8.943	0.449	0.592	42.20	
	SageAttention	7.243	0.433	0.744	49.79	
	SageAttn2-4b	7.352	0.433	0.725	49.23	
	SageAttn2-8b	7.242	0.432	0.745	49.60	
Model	Attention	CLIPSIM ↑	CLIP-T ↑	VQA-a ↑	VQA-t ↑	FScore ↑
CogvideoX (1.5-5B)	Full-Precision	0.1778	0.9979	70.231	70.928	2.507
	HadmdAttn	0.1576	0.9933	8.990	2.299	X
	SmoothAttn	0.1559	0.9950	8.812	2.277	X
	SageAttention	X	X	X	X	X
	FlashAttn3-fp8	0.1562	0.9918	6.531	2.181	X
	SageAttn2-4b	0.1721	0.9978	57.729	52.989	2.884
	SageAttn2-8b	0.1775	0.9980	69.492	74.415	2.487
Hunyuan Video	Full-Precision	0.1783	0.9995	82.516	75.934	0.604
	HadmdAttn	0.1727	0.9989	7.514	0.762	0.175
	SmoothAttn	0.1739	0.9988	6.987	0.609	0.148
	SageAttention	0.1786	0.9995	82.496	79.843	0.597
	FlashAttn3-fp8	0.1742	0.9941	4.433	1.460	X
	SageAttn2-4b	0.1751	0.9995	81.478	65.371	0.610
	SageAttn2-8b	0.1782	0.9996	81.786	75.354	0.586
Mochi	Full-Precision	0.1798	0.9986	45.549	65.416	1.266
	HadmdAttn	0.1733	0.9980	9.053	25.133	0.704
	SmoothAttn	0.1687	0.9978	3.383	3.480	0.241
	SageAttention	0.1800	0.9987	48.707	63.763	1.269
	FlashAttn3-fp8	0.1762	0.9982	14.964	13.711	0.457
	SageAttn2-4b	0.1783	0.9986	35.955	43.735	1.137
	SageAttn2-8b	0.1797	0.9986	46.760	64.901	1.255
Model	Attention	FID ↓	sFID ↓	CLIP ↑	IR ↑	
Flux	Full-Precision	10.960	16.648	26.180	1.009	
	HadmdAttn	11.353	18.495	26.123	0.965	
	SmoothAttn	11.149	19.017	26.109	0.959	
	SageAttention	10.944	16.641	26.171	1.008	
	SageAttn2-4b	10.577	17.497	26.141	0.998	
	SageAttn2-8b	10.927	16.723	26.175	1.009	
Stable-Dif fusion3.5	Full-Precision	14.105	15.646	25.505	0.902	
	HadmdAttn	14.259	15.909	25.513	0.886	
	SmoothAttn	14.161	15.649	25.510	0.887	
	SageAttention	14.140	15.678	25.503	0.902	
	SageAttn2-4b	14.097	15.397	25.487	0.895	
	SageAttn2-8b	14.106	15.647	25.499	0.901	

shown in Table 3 using CUDA.

Baselines. (1) SmoothAttn. Following Qserve (Lin et al., 2024), we apply smooth quant for Q, K with smoothing factor $\alpha = 0.5$. (2) HadmdAttn. Following Quarot (Ashkboos et al., 2024), we apply random Hadamard transformation for Q, K before INT4 quantization. (3) SageAttention (Zhang et al., 2025), which uses smoothing K , INT8 per-block quantization for Q, K , and FP16 for P, V . (4) FlashAttn3 (fp8), the FP8 version of FlashAttention3, which only runs on Hopper GPUs.

Table 4. Average accuracy across all layers of CogvideoX using different smoothing methods.

Method	CosSim \uparrow	Relative L1 \downarrow	RMSE \downarrow
None	80.04%	0.3906	0.2223
HadmdAttn	79.77%	0.3782	0.2180
SmoothAttn	90.21%	0.3383	0.1952
Smooth K	98.07%	0.1493	0.0743
Smooth Q	98.30%	0.1250	0.0712
Smooth Q+K	99.46%	0.0648	0.0334

Table 5. End-to-end metrics comparison, where Q, K are quantized into INT4, while \tilde{P}, V stay in full precision.

Q, K	Smooth (Q+K)	Llama3.1 (Lambda) \uparrow	Llama3.1 (WikiText) \downarrow	CogVideoX (vqa-t) \uparrow
Full-Precision	-	81.5%	6.013	75.360
INT4	\times	72.6%	11.698	24.670
Quantization	\checkmark	80.8%	6.219	75.147

Table 6. Average accuracy across all layers of CogvideoX using different quantization granularities.

Method	Cos Sim \uparrow	Relative L1 \downarrow	RMSE \downarrow
Per-token	99.45%	0.0649	0.0335
Per-thread	99.45%	0.0622	0.0313
Per-block	98.03%	0.1492	0.0744
Per-tensor	97.15%	0.1800	0.0865

Table 7. Average accuracy using different data types of (\tilde{P}, V) across all layers of CogvideoX, where (Q, K) are smoothed.

Q, K	\tilde{P}, V	Cos Sim \uparrow	Relative L1 \downarrow	RMSE \downarrow
INT4	INT8	77.05%	0.5618	0.5044
	E5M2	99.20%	0.0905	0.0903
	E4M3	99.44%	0.0683	0.0347
	FP16	99.45%	0.0649	0.0335

Table 8. End-to-end generation latency using SageAttention2 (The latency of Llama3.1 is the time to first token generation using different sequence lengths).

Model	GPU	Original	SageAttn 2-8b	SageAttn 2-4b
CogvideoX (2B)	RTX4090	86 s	54 s	52 s
CogvideoX (1.5-5B)	RTX4090	1040 s	577 s	555 s
HunyuanVideo	L20	2221 s	1486 s	1435 s
Mochi	L20	2336 s	1316 s	1190 s
Llama3.1 (48K token)	RTX4090	9.2 s	5.7 s	5.6 s
Llama3.1 (100K token)	L20	39.9 s	25.4 s	23.2 s

4.2. Speed and Accuracy of Kernels

Kernel Speed. We compare the Speed of SageAttention2 against baselines using configurations with headdim=64 and headdim=128, both with and without Causal Mask (Vaswani, 2017). Specifically, Fig. 5 shows the speed across varying sequence lengths on RTX4090, indicating that SageAttn2-4b and SageAttn2-8b are approximately 3x and 2.7x faster than FlashAttention2, and about 4.5x and 4x faster than xformers, respectively. Fig. 9, 10, 11, 12, 13, 14, and 15 in Appendix A.2 show more kernel speed comparison on RTX4090, L20, H20, H100 GPUs.

Accuracy. Table 4 and 17 show the average accuracy of different methods with INT4 Q, K and FP8 P, V across all layers of CogvideoX. The results indicate the accuracy of SageAttn2-4b is superior to other baselines.

4.3. End-to-end Performance

Metrics loss. We assessed the end-to-end metrics of various models using SageAttention2 compared to baselines. Detailed evaluation results are presented in Table 2. The results indicate that SageAttn2-4b outperforms all baselines and maintains most of the end-to-end accuracy across all models. Additionally, SageAttn2-8b incurs almost no metrics loss across various models. More experiment results on other models are shown in Appendix A.7.

Visible image and video examples. Fig.6 and Fig. 8 in Appendix A.1 show some visible comparison examples from HunyuanVideo, Mochi and CogvideoX (1.5-5B). We can observe that SageAttn2-8b does not introduce any visible differences compared to full-precision attention, whereas SageAttn2-4b has minor differences but is much better than the baselines.

End-to-end speedup. We compared the original generation latency and the latency using SageAttention2 for models with long sequence lengths in Table 8, observing significant speedup effects. For instance, SageAttention2 achieved a **1.8x** speedup in CogvideoX (1.5-5B) without any metrics loss (SageAttn2-8b). SageAttn2-4b further accelerated these models but with a little metrics loss.

4.4. Ablation Study

Overhead of techniques we proposed. As shown in Table 18, the overhead on kernel speed of per-thread quantization, smoothing Q, and two-level accumulation are 0.35%, 3.7%, and 0% compared to the attention kernel.

Benefit of smoothing V. The experiment showing the benefit of smoothing V is shown in Appendix. A.4.

5. Conclusion

We introduce SageAttention2, an efficient and accurate quantized attention. First, we propose to quantize matrixes (Q, K) in a thread-level granularity and (\tilde{P}, V) to FP8. Second, we propose a method to smooth Q , enhancing the accuracy of QK^\top . Third, we propose a two-level accumulation strategy to enhance the accuracy of FP8 $\tilde{P}V$. SageAttention2 is faster than FlashAttention2 and xformers by approximately **3x** and **4.5x**, respectively. Moreover, SageAttention2 matches the speed of FlashAttention3(fp8) on the Hopper GPUs, but offers significantly higher accuracy. Extensive testing confirms that our approach maintains end-to-end metrics across language, image, and video generation models.

References

- Ashkboos, S., Mohtashami, A., Croci, M. L., Li, B., Cameron, P., Jaggi, M., Alistarh, D., Hoefler, T., and Hensman, J. Quarot: Outlier-free 4-bit inference in rotated LLMs. In *The Thirty-eighth Annual Conference on Neural Information Processing Systems*, 2024.
- Bai, Y., Lv, X., Zhang, J., Lyu, H., Tang, J., Huang, Z., Du, Z., Liu, X., Zeng, A., Hou, L., Dong, Y., Tang, J., and Li, J. LongBench: A bilingual, multitask benchmark for long context understanding. In *Proceedings of the 62nd Annual Meeting of the Association for Computational Linguistics (Volume 1: Long Papers)*, pp. 3119–3137, 2024.
- Black Forest Labs. Flux. <https://github.com/black-forest-labs/flux>, 2023.
- Chen, Y., Qian, S., Tang, H., Lai, X., Liu, Z., Han, S., and Jia, J. Longlora: Efficient fine-tuning of long-context large language models. In *The International Conference on Learning Representations*, 2024.
- Choromanski, K. M., Likhoshesterov, V., Dohan, D., Song, X., Gane, A., Sarlos, T., Hawkins, P., Davis, J. Q., Mohiuddin, A., Kaiser, L., Belanger, D. B., Colwell, L. J., and Weller, A. Rethinking attention with performers. In *International Conference on Learning Representations*, 2021.
- Chu, X., Tian, Z., Wang, Y., Zhang, B., Ren, H., Wei, X., Xia, H., and Shen, C. Twins: Revisiting the design of spatial attention in vision transformers. In Beygelzimer, A., Dauphin, Y., Liang, P., and Vaughan, J. W. (eds.), *Advances in Neural Information Processing Systems*, 2021.
- Dao, T. Flashattention-2: Faster attention with better parallelism and work partitioning. In *The Twelfth International Conference on Learning Representations*, 2024.
- Dao, T., Fu, D. Y., Ermon, S., Rudra, A., and Re, C. Flashattention: Fast and memory-efficient exact attention with IO-awareness. In Oh, A. H., Agarwal, A., Belgrave, D., and Cho, K. (eds.), *Advances in Neural Information Processing Systems*, 2022.
- DeepSeek-AI, Liu, A., Feng, B., Xue, B., Wang, B., Wu, B., Lu, C., Zhao, C., Deng, C., Zhang, C., Ruan, C., Dai, D., Guo, D., Yang, D., Chen, D., Ji, D., Li, E., Lin, F., Dai, F., Luo, F., Hao, G., Chen, G., Li, G., Zhang, H., Bao, H., Xu, H., Wang, H., Zhang, H., Ding, H., Xin, H., Gao, H., Li, H., Qu, H., Cai, J. L., Liang, J., Guo, J., Ni, J., Li, J., Wang, J., Chen, J., Chen, J., Yuan, J., Qiu, J., Li, J., Song, J., Dong, K., Hu, K., Gao, K., Guan, K., Huang, K., Yu, K., Wang, L., Zhang, L., Xu, L., Xia, L., Zhao, L., Wang, L., Zhang, L., Li, M., Wang, M., Zhang, M., Zhang, M., Tang, M., Li, M., Tian, N., Huang, P., Wang, P., Zhang, P., Wang, Q., Zhu, Q., Chen, Q., Du, Q., Chen, R. J., Jin, R. L., Ge, R., Zhang, R., Pan, R., Wang, R., Xu, R., Zhang, R., Chen, R., Li, S. S., Lu, S., Zhou, S., Chen, S., Wu, S., Ye, S., Ye, S., Ma, S., Wang, S., Zhou, S., Yu, S., Zhou, S., Pan, S., Wang, T., Yun, T., Pei, T., Sun, T., Xiao, W. L., Zeng, W., Zhao, W., An, W., Liu, W., Liang, W., Gao, W., Yu, W., Zhang, W., Li, X. Q., Jin, X., Wang, X., Bi, X., Liu, X., Wang, X., Shen, X., Chen, X., Zhang, X., Chen, X., Nie, X., Sun, X., Wang, X., Cheng, X., Liu, X., Xie, X., Liu, X., Yu, X., Song, X., Shan, X., Zhou, X., Yang, X., Li, X., Su, X., Lin, X., Li, Y. K., Wang, Y. Q., Wei, Y. X., Zhu, Y. X., Zhang, Y., Xu, Y., Xu, Y., Huang, Y., Li, Y., Zhao, Y., Sun, Y., Li, Y., Wang, Y., Yu, Y., Zheng, Y., Zhang, Y., Shi, Y., Xiong, Y., He, Y., Tang, Y., Piao, Y., Wang, Y., Tan, Y., Ma, Y., Liu, Y., Guo, Y., Wu, Y., Ou, Y., Zhu, Y., Wang, Y., Gong, Y., Zou, Y., He, Y., Zha, Y., Xiong, Y., Ma, Y., Yan, Y., Luo, Y., You, Y., Liu, Y., Zhou, Y., Wu, Z. F., Ren, Z. Z., Ren, Z., Sha, Z., Fu, Z., Xu, Z., Huang, Z., Zhang, Z., Xie, Z., Zhang, Z., Hao, Z., Gou, Z., Ma, Z., Yan, Z., Shao, Z., Xu, Z., Wu, Z., Zhang, Z., Li, Z., Gu, Z., Zhu, Z., Liu, Z., Li, Z., Xie, Z., Song, Z., Gao, Z., and Pan, Z. Deepseek-v3 technical report. *arXiv preprint arXiv:2412.19437*, 2024.
- Deng, J., Dong, W., Socher, R., Li, L.-J., Li, K., and Fei-Fei, L. Imagenet: A large-scale hierarchical image database. In *2009 IEEE conference on computer vision and pattern recognition*, pp. 248–255. Ieee, 2009.
- Dubey, A., Jauhri, A., Pandey, A., Kadian, A., Al-Dahle, A., Letman, A., Mathur, A., Schelten, A., Yang, A., Fan, A., et al. The llama 3 herd of models. *arXiv preprint arXiv:2407.21783*, 2024.
- Fu, T., Huang, H., Ning, X., Zhang, G., Chen, B., Wu, T., Wang, H., Huang, Z., Li, S., Yan, S., Dai, G., Yang, H., and Wang, Y. Moa: Mixture of sparse attention for automatic large language model compression. *arXiv preprint arXiv:2406.14909*, 2024.

- Gao, Y., Zeng, Z., Du, D., Cao, S., So, H. K.-H., Cao, T., Yang, F., and Yang, M. Seerattention: Learning intrinsic sparse attention in your llms. *arXiv preprint arXiv:2410.13276*, 2024.
- GLM, T., Zeng, A., Xu, B., Wang, B., Zhang, C., Yin, D., Rojas, D., Feng, G., Zhao, H., Lai, H., Yu, H., Wang, H., Sun, J., Zhang, J., Cheng, J., Gui, J., Tang, J., Zhang, J., Li, J., Zhao, L., Wu, L., Zhong, L., Liu, M., Huang, M., Zhang, P., Zheng, Q., Lu, R., Duan, S., Zhang, S., Cao, S., Yang, S., Tam, W. L., Zhao, W., Liu, X., Xia, X., Zhang, X., Gu, X., Lv, X., Liu, X., Liu, X., Yang, X., Song, X., Zhang, X., An, Y., Xu, Y., Niu, Y., Yang, Y., Li, Y., Bai, Y., Dong, Y., Qi, Z., Wang, Z., Yang, Z., Du, Z., Hou, Z., and Wang, Z. Chatglm: A family of large language models from glm-130b to glm-4 all tools. *arXiv preprint arXiv:2406.12793*, 2024.
- Hendrycks, D., Burns, C., Basart, S., Zou, A., Mazeika, M., Song, D., and Steinhardt, J. Measuring massive multitask language understanding. *arXiv preprint arXiv:2009.03300*, 2020.
- Hendrycks, D., Basart, S., Mu, N., Kadavath, S., Wang, F., Dorundo, E., Desai, R., Zhu, T., Parajuli, S., Guo, M., et al. The many faces of robustness: A critical analysis of out-of-distribution generalization. In *Proceedings of the IEEE/CVF international conference on computer vision*, pp. 8340–8349, 2021.
- Hessel, J., Holtzman, A., Forbes, M., Le Bras, R., and Choi, Y. Clipscore: A reference-free evaluation metric for image captioning. In *Proceedings of the 2021 Conference on Empirical Methods in Natural Language Processing*, pp. 7514–7528, 2021.
- Heusel, M., Ramsauer, H., Unterthiner, T., Nessler, B., and Hochreiter, S. Gans trained by a two time-scale update rule converge to a local nash equilibrium. *Advances in neural information processing systems*, 30, 2017.
- Jelinek, F., Mercer, R. L., Bahl, L. R., and Baker, J. K. Perplexity—a measure of the difficulty of speech recognition tasks. *The Journal of the Acoustical Society of America*, 62(S1):S63–S63, 1977.
- Jiang, H., LI, Y., Zhang, C., Wu, Q., Luo, X., Ahn, S., Han, Z., Abdi, A. H., Li, D., Lin, C.-Y., Yang, Y., and Qiu, L. MInference 1.0: Accelerating pre-filling for long-context LLMs via dynamic sparse attention. In *The Thirty-eighth Annual Conference on Neural Information Processing Systems*, 2024.
- Kamradt, G. Llmtest needle in a haystack - pressure testing llms. https://github.com/gkamradt/LLMTest_NeedleInAHaystack, 2023.
- Katharopoulos, A., Vyas, A., Pappas, N., and Fleuret, F. Transformers are rnns: Fast autoregressive transformers with linear attention. In *International conference on machine learning*, pp. 5156–5165. PMLR, 2020.
- Kong, W., Tian, Q., Zhang, Z., Min, R., Dai, Z., Zhou, J., Xiong, J., Li, X., Wu, B., Zhang, J., Wu, K., Lin, Q., Wang, A., Wang, A., Li, C., Huang, D., Yang, F., Tan, H., Wang, H., Song, J., Bai, J., Wu, J., Xue, J., Wang, J., Yuan, J., Wang, K., Liu, M., Li, P., Li, S., Wang, W., Yu, W., Deng, X., Li, Y., Long, Y., Chen, Y., Cui, Y., Peng, Y., Yu, Z., He, Z., Xu, Z., Zhou, Z., Xu, Z., Tao, Y., Lu, Q., Liu, S., Zhou, D., Wang, H., Yang, Y., Wang, D., Liu, Y., Jiang, J., and Zhong, C. Hunyuanvideo: A systematic framework for large video generative models. *arXiv preprint arXiv:2412.03603*, 2024.
- Lefaudeaux, B., Massa, F., Liskovich, D., Xiong, W., Caggiano, V., Naren, S., Xu, M., Hu, J., Tintore, M., Zhang, S., Labatut, P., Haziza, D., Wehrstedt, L., Reizenstein, J., and Sizov, G. xformers: A modular and hackable transformer modelling library. <https://github.com/facebookresearch/xformers>, 2022.
- Li, D., Kamko, A., Akhgari, E., Sabet, A., Xu, L., and Doshi, S. Playground v2.5: Three insights towards enhancing aesthetic quality in text-to-image generation. *arXiv preprint arXiv:2402.17245*, 2024.
- Li, K., Wang, Y., Peng, G., Song, G., Liu, Y., Li, H., and Qiao, Y. Uniformer: Unified transformer for efficient spatial-temporal representation learning. In *International Conference on Learning Representations*, 2022.
- Lin, Y., Tang, H., Yang, S., Zhang, Z., Xiao, G., Gan, C., and Han, S. Qserve: W4a8kv4 quantization and system co-design for efficient llm serving. *arXiv preprint arXiv:2405.04532*, 2024.
- Liu, Y., Cun, X., Liu, X., Wang, X., Zhang, Y., Chen, H., Liu, Y., Zeng, T., Chan, R., and Shan, Y. Evalcrafter: Benchmarking and evaluating large video generation models. In *Proceedings of the IEEE/CVF Conference on Computer Vision and Pattern Recognition*, pp. 22139–22149, 2024.
- Liu, Z., Lin, Y., Cao, Y., Hu, H., Wei, Y., Zhang, Z., Lin, S., and Guo, B. Swin transformer: Hierarchical vision transformer using shifted windows. In *Proceedings of the IEEE/CVF international conference on computer vision*, pp. 10012–10022, 2021.
- Merity, S., Xiong, C., Bradbury, J., and Socher, R. Pointer sentinel mixture models. In *International Conference on Learning Representations*, 2022.

- Milakov, M. and Gimelshein, N. Online normalizer calculation for softmax. *arXiv preprint arXiv:1805.02867*, 2018.
- NVIDIA. Parallel thread execution isa version 8.5. <https://docs.nvidia.com/cuda/parallel-thread-execution/>.
- NVIDIA. CUTLASS: CUDA Templates for Linear Algebra Subroutines and Solvers. GitHub repository, 2023. URL <https://github.com/NVIDIA/cutlass>.
- Paperno, D., Kruszewski, G., Lazaridou, A., Pham, N.-Q., Bernardi, R., Pezzelle, S., Baroni, M., Boleda, G., and Fernández, R. The lambada dataset: Word prediction requiring a broad discourse context. In *Proceedings of the 54th Annual Meeting of the Association for Computational Linguistics (Volume 1: Long Papers)*, pp. 1525–1534, 2016.
- Salimans, T., Goodfellow, I., Zaremba, W., Cheung, V., Radford, A., and Chen, X. Improved techniques for training gans. *Advances in neural information processing systems*, 29, 2016.
- Shah, J., Bikshandi, G., Zhang, Y., Thakkar, V., Ramani, P., and Dao, T. Flashattention-3: Fast and accurate attention with asynchrony and low-precision. In *The Thirty-eighth Annual Conference on Neural Information Processing Systems*, 2024.
- Stability AI. Introducing stable diffusion 3.5. <https://stability.ai/news/introducing-stable-diffusion-3-5>, 2023.
- Team, G. Mochi 1. <https://github.com/genmoai/models>, 2024.
- Touvron, H., Martin, L., Stone, K., Albert, P., Almahairi, A., Babaei, Y., Bashlykov, N., Batra, S., Bhargava, P., Bhosale, S., et al. Llama 2: Open foundation and fine-tuned chat models. *arXiv preprint arXiv:2307.09288*, 2023.
- Vaswani, A. Attention is all you need. *Advances in Neural Information Processing Systems*, 2017.
- Venkataramanan, S., Ghodrati, A., Asano, Y. M., Porikli, F., and Habibi, A. Skip-attention: Improving vision transformers by paying less attention. In *The Twelfth International Conference on Learning Representations*, 2024.
- Wang, H., Ge, S., Lipton, Z., and Xing, E. P. Learning robust global representations by penalizing local predictive power. *Advances in Neural Information Processing Systems*, 32, 2019.
- Wang, S., Li, B. Z., Khabsa, M., Fang, H., and Ma, H. Linformer: Self-attention with linear complexity. *arXiv preprint arXiv:2006.04768*, 2020.
- Wightman, R. Pytorch image models. <https://github.com/rwightman/pytorch-image-models>, 2019.
- Wu, H., Zhang, E., Liao, L., Chen, C., Hou, J., Wang, A., Sun, W., Yan, Q., and Lin, W. Exploring video quality assessment on user generated contents from aesthetic and technical perspectives. In *Proceedings of the IEEE/CVF International Conference on Computer Vision*, pp. 20144–20154, 2023.
- Xiao, C., Zhang, P., Han, X., Xiao, G., Lin, Y., Zhang, Z., Liu, Z., and Sun, M. Infilmm: Training-free long-context extrapolation for llms with an efficient context memory. In *First Workshop on Long-Context Foundation Models@ICML 2024*, 2024a.
- Xiao, G., Lin, J., Seznec, M., Wu, H., Demouth, J., and Han, S. Smoothquant: Accurate and efficient post-training quantization for large language models. In *International Conference on Machine Learning*, pp. 38087–38099. PMLR, 2023.
- Xiao, G., Tian, Y., Chen, B., Han, S., and Lewis, M. Efficient streaming language models with attention sinks. In *The Twelfth International Conference on Learning Representations*, 2024b.
- Xu, J., Liu, X., Wu, Y., Tong, Y., Li, Q., Ding, M., Tang, J., and Dong, Y. Imagereward: Learning and evaluating human preferences for text-to-image generation. In *Thirty-seventh Conference on Neural Information Processing Systems*, 2023.
- Yang, Z., Teng, J., Zheng, W., Ding, M., Huang, S., Xu, J., Yang, Y., Hong, W., Zhang, X., Feng, G., et al. Cogvideox: Text-to-video diffusion models with an expert transformer. In *The Thirteenth International Conference on Learning Representations*, 2025.
- Yu, W., Luo, M., Zhou, P., Si, C., Zhou, Y., Wang, X., Feng, J., and Yan, S. Metaformer is actually what you need for vision. In *Proceedings of the IEEE/CVF conference on computer vision and pattern recognition*, pp. 10819–10829, 2022.
- Zhang, J., Wei, J., Zhang, P., Chen, J., and Zhu, J. Sageattention: Accurate 8-bit attention for plug-and-play inference acceleration. In *The International Conference on Learning Representations*, 2025.
- Zhang, X., Chen, Y., Hu, S., Xu, Z., Chen, J., Hao, M., Han, X., Thai, Z., Wang, S., Liu, Z., and Sun, M. ∞ Bench: Extending long context evaluation beyond 100K tokens.

In Ku, L.-W., Martins, A., and Srikumar, V. (eds.), *Proceedings of the 62nd Annual Meeting of the Association for Computational Linguistics (Volume 1: Long Papers)*, pp. 15262–15277, 2024.

Zhao, T., Fang, T., Huang, H., Liu, E., Wan, R., Soedarmadji, W., Li, S., Lin, Z., Dai, G., Yan, S., Yang, H., et al. Vedit-q: Efficient and accurate quantization of diffusion transformers for image and video generation. In *International Conference on Learning Representations*, 2025.

Zheng, Z., Peng, X., Yang, T., Shen, C., Li, S., Liu, H., Zhou, Y., Li, T., and You, Y. Open-sora: Democratizing efficient video production for all. *arXiv preprint arXiv:2412.20404*, 2024.

A. Appendix

A.1. Visible Comparison Exmaples

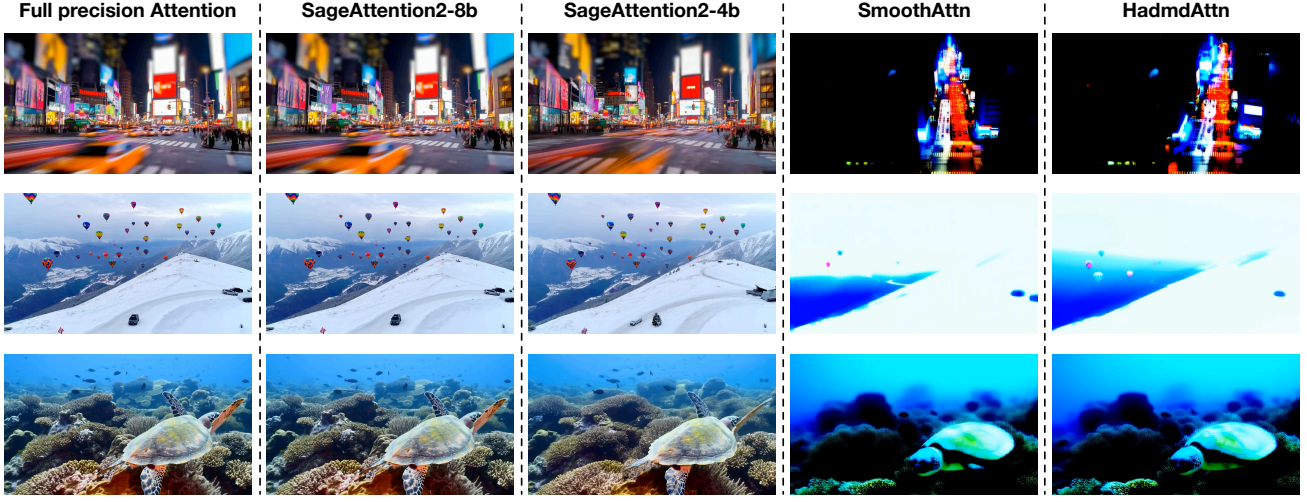


Figure 6. Comparison examples from HunyuanVideo, prompts are sampled from open-sora prompt sets.

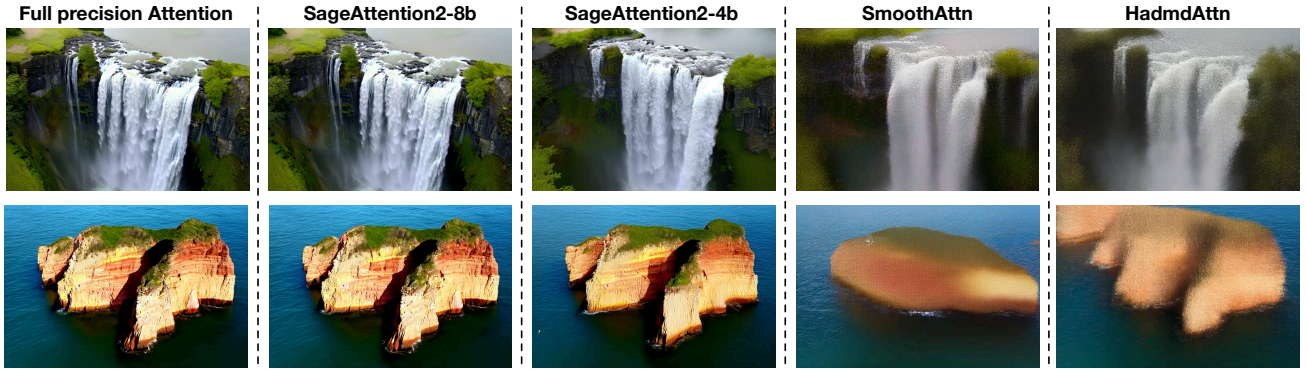


Figure 7. Comparison examples from CogvideoX (2B), prompts are sampled from open-sora prompt sets.

A.2. Additional Kernel Speed Comparison

Fig. 9, 10, 11, 12, 13, 14, and 15 compare the speed of SageAttention2 against baselines using configurations with headdim=64 and headdim=128, both with and without Causal Mask (Vaswani, 2017), on RTX4090, L20, H100, and H20 GPUs.

Table 9 summarizes the performance gain of different attention methods against baselines on various modern GPUs.

Table 9. Speedup of different attention methods on various GPUs.

Method	3090	4090	A100	L40	L20	H100	H20
FlashAttention2	1.00	1.00	1.00	1.00	1.00	1.00	1.00
FlashAttention3	✗	✗	✗	✗	✗	1.37	1.57
FlashAttention3 (fp8)	✗	✗	✗	✗	✗	2.63	3.06
SageAttention1	1.97	1.96	1.37	1.45	1.24	1.53	1.52
SageAttention2	✗	2.93	✗	2.60	2.46	2.61	3.12

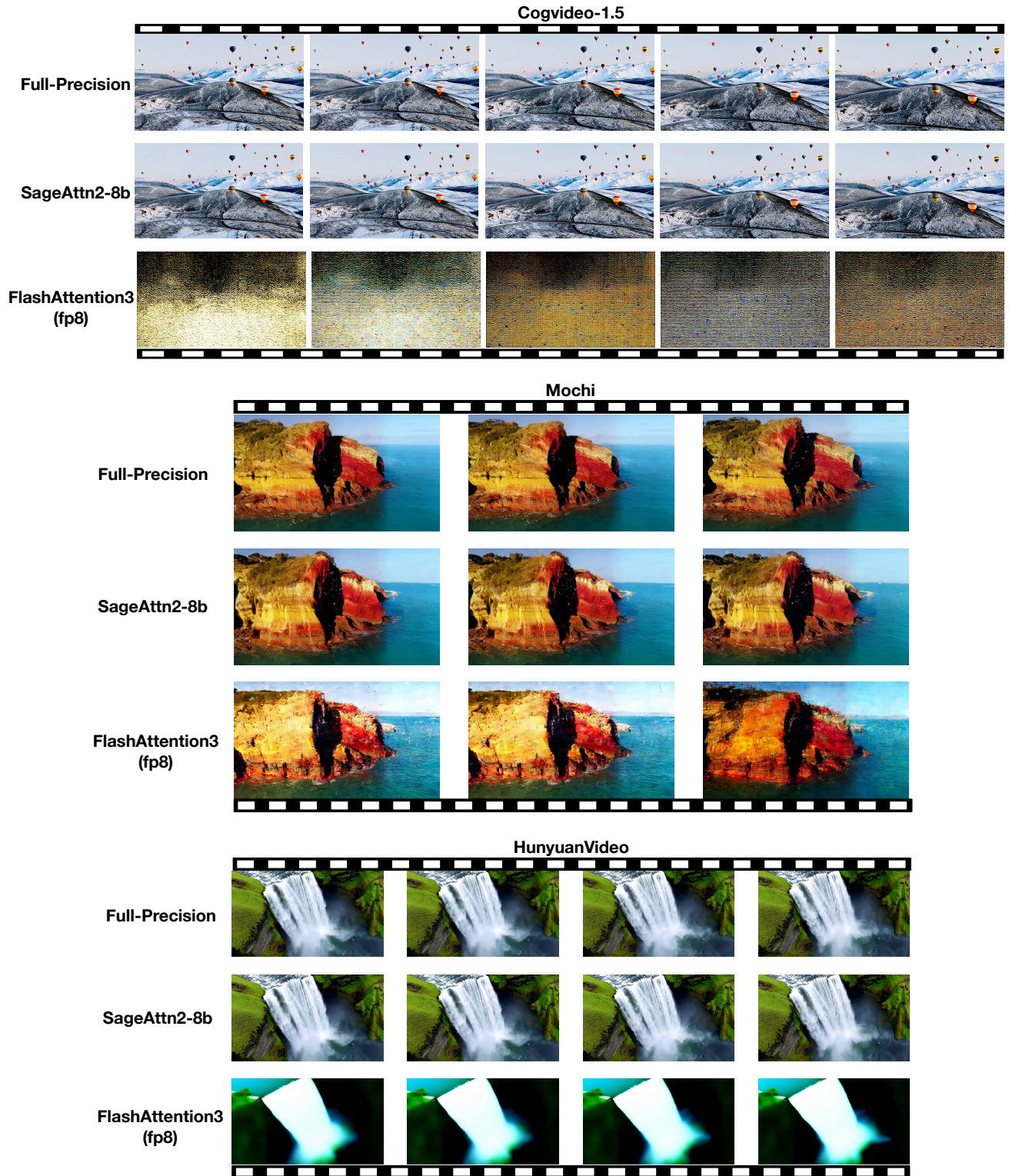


Figure 8. A comparison example using SageAttn2-8b and FlashAttention3 on CogvideoX-1.5, Mochi and HunyuanVideo.

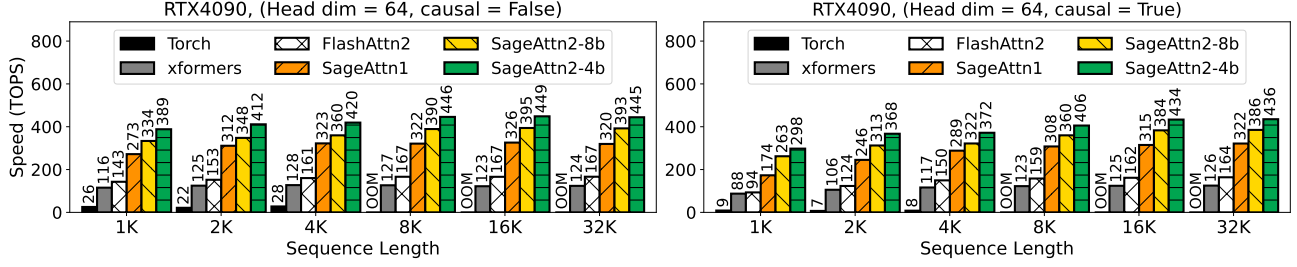


Figure 9. Speed comparison between SageAttention2 and baselines (RTX4090, headdim=64).

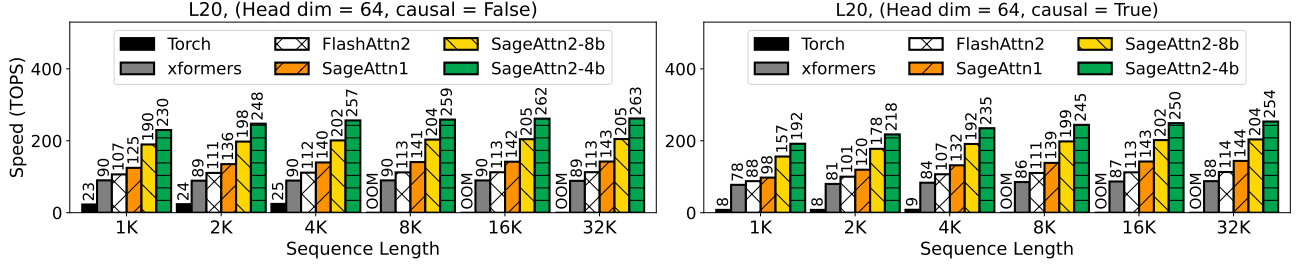


Figure 10. Speed comparison between SageAttention2 and baselines (L20, headdim=64).

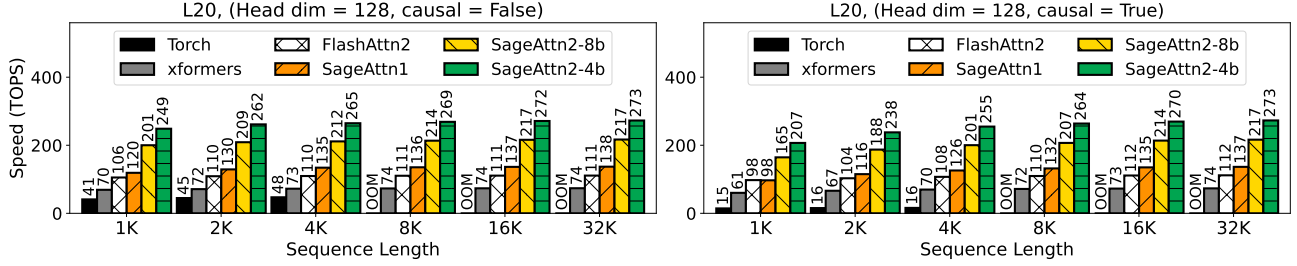


Figure 11. Speed comparison between SageAttention2 and baselines (L20, headdim=128).

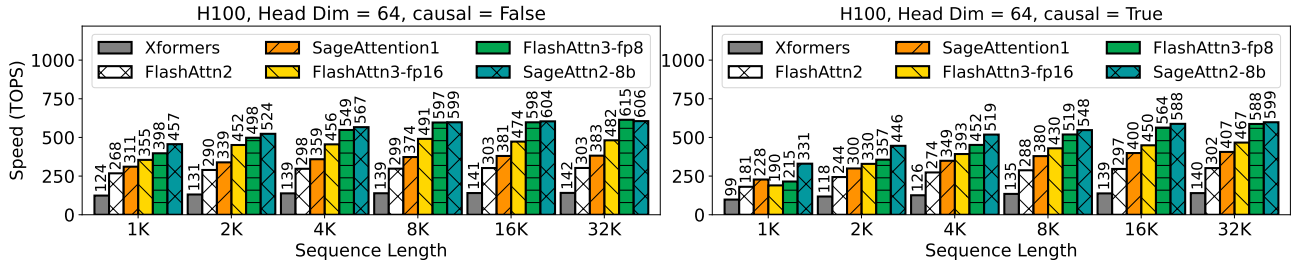


Figure 12. Speed comparison between SageAttention2 and baselines (H100, headdim=64).

 Table 10. An accuracy example on real tensors of CogvideoX model with or without smoothing V .

Smooth V	Cos Sim \uparrow	Relative L1 \downarrow	RMSE \downarrow
\times	98.25%	0.1980	0.2387
\checkmark	99.75%	0.0406	0.0773

A.3. Smoothing V

As shown in Fig. 16, this strategy could enhance the accuracy of FP22 for values in $\tilde{P}V$ for the following reasons: Each row of \tilde{P} spans a value range from 0 to 1, and each column of V in some models consistently features channel-wise biases

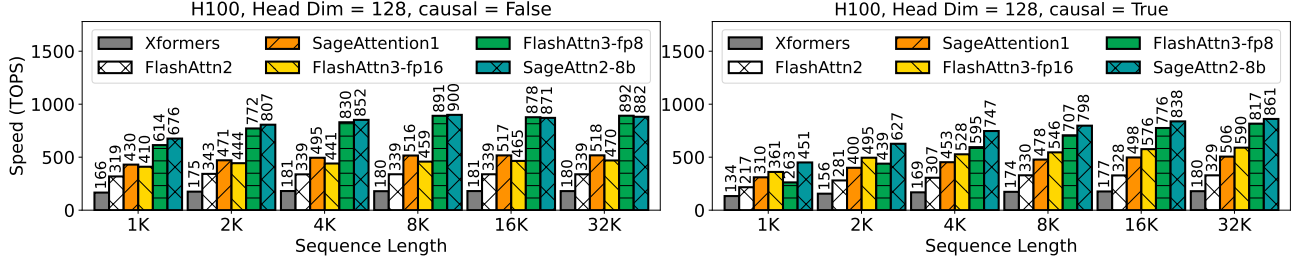


Figure 13. Speed comparison between SageAttention2 and baselines (H100, headdim=128).

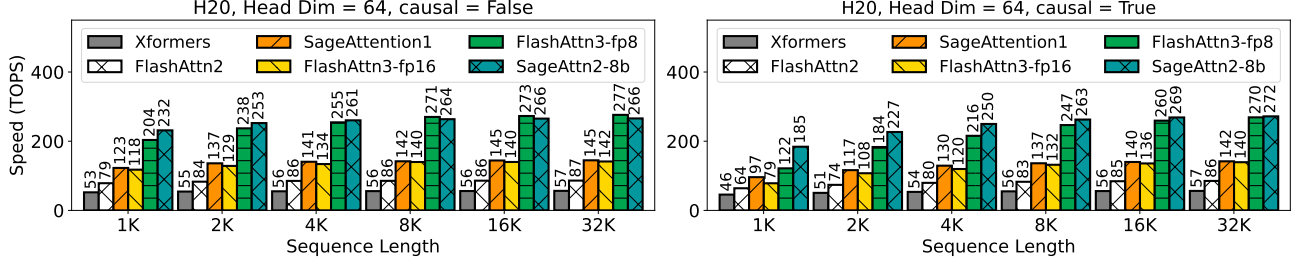


Figure 14. Speed comparison between SageAttention2 and baselines (H20, headdim=64).

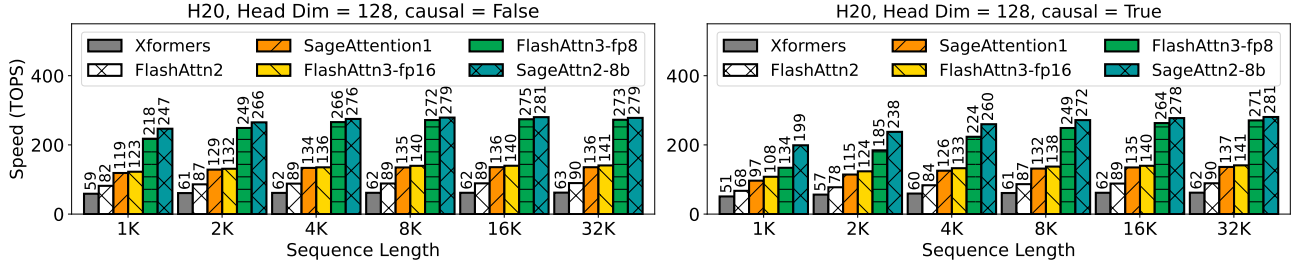
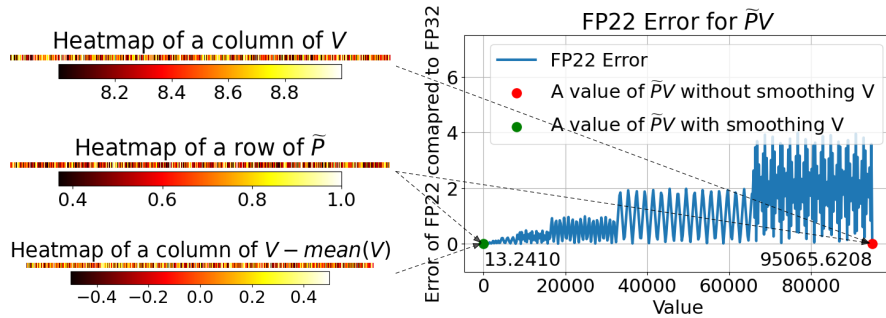


Figure 15. Speed comparison between SageAttention2 and baselines (H20, headdim=128).


 Figure 16. An example of dot product precision a row of \tilde{P} and a column of V presented by FP22 data type.

that are exclusively positive or negative, for instance, ranging between 8 and 9 in CogvideoX. Consequently, the values of $\tilde{P}V$ could be quite large. However, the floating-point number representation range is not uniform—it is denser near zero. Therefore, by subtracting the mean \vec{V}_m along the channel dimension from V , the values of $\tilde{P}V$ will be closer to zero, resulting in higher representational precision (see Fig. 16 for a visual demonstration). Additionally, to maintain the correctness of the attention computation, it is only necessary to add \vec{V}_m to the final calculation of O : $O = O + \vec{V}_m$. This is because the sum of each row of the \tilde{P} matrix equals 1, so $\tilde{P}\vec{V}_m = \vec{V}_m$. In other words, this method decomposes V

into two parts: \vec{V}_m and V . For V , it centers the values of each column around zero, which leads to the dot product result between a row from the quantized \tilde{P} matrix and a column from the quantized V matrix being closer to zero. This makes the representation of FP22 more accurate. Meanwhile, \vec{V}_m is retained in FP16 and added to O at the end without causing a loss of precision for the \vec{V}_m part.

A.4. Experiment of Smoothing V

Table 10 shows the attention accuracy on real tensors sampled from CogvideoX with and without smoothing V . It demonstrates that smoothing V could improve the accuracy of SageAttention2 when quantizing Q, K to INT4 and \tilde{P}, V to FP8.

A.5. Per-Thread Quantization Formulation

R\C	0	1	2	3	4	5	6	7
0	T0: {c0, c1}	T1: {c0, c1}	T2: {c0, c1}	T3: {c0, c1}				
1	T4: {c0, c1}	T5: {c0, c1}	T6: {c0, c1}	T7: {c0, c1}				
2								
7	T28: {c0, c1}	T29: {c0, c1}	T30: {c0, c1}	T31: {c0, c1}				
8	T0: {c2, c3}	T1: {c2, c3}	T2: {c2, c3}	T3: {c2, c3}				
9	T4: {c2, c3}	T5: {c2, c3}	T6: {c2, c3}	T7: {c2, c3}				
10								
..								
15	T28: {c2, c3}	T29: {c2, c3}	T30: {c2, c3}	T31: {c2, c3}				

Figure 17. Memory layout of INT4/INT8 tensor core for accumulator matrix C and D in $D = A * B + C$ among 32 threads (T0 ~ T31) in a warp. C and D is of shape 16x8. Each thread only holds 4 out of the 128 elements.

To further clarify the per-thread quantization, we first introduce the INT4 MMA instruction of Tensor Core, and then give the formulation of per-thread quantization.

Tensor cores, first introduced in NVIDIA’s Volta architecture, are specialized units designed for efficient matrix-multiply-and-accumulate (MMA) operations. Their usage significantly enhances computational efficiency and performance in AI and high-performance computing (HPC) workloads. Tensor cores compute small tiles of MMA operations, specifically $D = A * B + C$ on a warp (32 contiguous threads) basis. Each thread in the warp holds a fragment of input matrices and will get a fragment of output matrix as a computation result. The INT4_mma.m16n8k64 tensor core operation computes the product of a 16×64 INT4 matrix A and a 64×8 INT4 matrix B , both stored in registers. It accumulates the result into a 16×8 INT32 matrix C , also stored in registers, and returns the final product matrix D , which has the same shape (16×8), data type (INT32), and storage location (registers). Each thread holds only $\frac{1}{32}$ of the input and output data. Fig. 17 extracted from the PTX document (NVIDIA) shows the memory layout of matrix C and D among 32 threads in a warp. Each thread only holds 4 out of the 128 result elements.

$$\begin{aligned}
 i_{\delta q} &= \lfloor (n * 8 * c_w / b_q) \rfloor \\
 q_i[i_{\delta q}] &= \{8 \times (n \% 8) + \lfloor (n * \frac{c_w}{b_q}) \rfloor * \frac{b_q}{c_w}\}, n \in [0, N] \\
 \delta_Q[i_{\delta q}] &= \frac{\max(|Q[q_i[i_{\delta q}]]|)}{7} \\
 \hat{Q}[q_i[i_{\delta q}]] &= \left\lceil \frac{Q[q_i[i_{\delta q}]]}{\delta_Q[i_{\delta q}]} \right\rceil
 \end{aligned}$$

$$\begin{aligned}
 i_{\delta k} &= \lfloor (n * 4 / b_k) \rfloor \\
 k_n[i_{\delta k}] &= \{8 \times (n \% 8) + \lfloor n / b_k \rfloor * b_k\} \cup \\
 &\quad \{8 \times (n \% 8) + 1 + \lfloor n / b_k \rfloor * b_k\}, \quad n \in [0, N] \\
 \delta_K[i_{\delta k}] &= \frac{\max(|K[k_n[i_{\delta k}]]|)}{7} \\
 \hat{K}[k_n[i_{\delta k}]] &= \left\lceil \frac{K[k_n[i_{\delta k}]]}{\delta_K[i_{\delta k}]} \right\rceil
 \end{aligned} \tag{3}$$

In Eq. 3, c_w is the count of GPU Warps. b_q and b_k are the block size of Q , K . n is the token index of Q , K .

By ensuring results held by each thread share a common dequantization scale (belong to the same quantization group), we can avoid the overhead associated with per-token quantization. Leveraging this observation, we design per-thread quantization, as shown in Fig. 4. For typical block size of $b_q = 128$, $b_k = 64$ and warp number $c_w = 4$ (as used in FlashAttention2), each warp processes a tile of 32 query tokens and 64 key tokens. Query tokens $i, 8 + i, 16 + i, 24 + i$ ($i = 0, 1, \dots, 7$) can be made into one quantization group and key tokens $j, 1 + j, 8 + j, 9 + j, \dots, 56 + j, 57 + j$ ($j = 0, 1, 2, 3$) can be made into one quantization group. This design aligns with the memory layout of output matrix D of tensor core shown in Fig. 17, ensuring that each thread only needs one Q scale and one K scale for dequantization.

As a result, this approach creates 32 quantization groups for Q (8 for each of the 4 warps) and 4 quantization groups for K in a 128×64 block, providing $32 \times$ and $4 \times$ finer granularity compared to per-block quantization for query tokens and key tokens, respectively. Table 6 and Table 15 show the accuracy gains by using per-thread quantization. Per-thread quantization achieves accuracy that closely matches per-token quantization, without introducing any kernel speed degradation (see Fig. 18).

A.6. Datasets and Metrics in Experiments

Datasets. Text-to-text models are evaluated on four zero-shot tasks: WikiText (Merity et al., 2022) to assess the model’s prediction confidence, LAMBADA (Paperno et al., 2016) evaluate contextual understanding, MMLU (Hendrycks et al., 2020) for measuring knowledge across various subjects, and Longbench (Bai et al., 2024) for comprehensive assessment of long context understanding capabilities. Text-to-video models are evaluated using the open-sora (Zheng et al., 2024) prompt sets. Text-to-image models are assessed on MJHQ-30K (Li et al., 2024). TIMM is evaluated on three image datasets: ImageNet (Deng et al., 2009), ImageNet-Sketch (Sketch) (Wang et al., 2019), and ImageNet-Rendition (ImageNet-r) (Hendrycks et al., 2021).

End-to-end metrics. For text-to-text models, we use perplexity (ppl.) (Jelinek et al., 1977) for WikiText, Accuracy (Acc.) for LAMBADA and MMLU, and Longbench score (Bai et al., 2024). For text-to-video models, following Zhao et al. (2025), we evaluate the quality of generated videos on five metrics: CLIPSIM and CLIP-Temp (CLIP-T) (Liu et al., 2024) to measure the text-video alignment; (VQA-a) and (VQA-t) to assess the video aesthetic and technical quality, respectively; and Flow-score (FScore) for temporal consistency (Wu et al., 2023). For text-to-image models, generated images are compared with the images in MJHQ-30K dataset in three aspects: FID (Heusel et al., 2017) and sFID (Salimans et al., 2016) for fidelity evaluation, *Clipscore* (CLIP) (Hessel et al., 2021) for text-image alignment, and *ImageReward* (IR) (Xu et al., 2023) for human preference. For TIMM, we use classification accuracy.

Accuracy metrics. We use three metrics to assess the accuracy of quantized attention output O' compared to attention output in full-precision O : First, we flatten O' and O into vectors in the shape of $1 \times n$. Then, Cosine similarity: $CosSim = \sum OO' / \sqrt{\sum O^2} \sqrt{\sum O'^2}$, Relative L1 distance: $L1 = \sum |O - O'| / \sum |O|$, Root mean square error: $RMSE = \sqrt{(1/n) \sum (O - O')^2}$.

A.7. Additional Experiments and Analysis

Additional Results. Table 11, 12 and 13 show results of SageAttention2 and other baselines on Llama2 (7B), CogvideoX (2B) and TIMM.

Results of Super-Long Context. We further conduct experiments on super-long context using Llama-3-262k (8B)¹ on InfiniBench (Zhang et al., 2024) and Needle-in-a-Haystack (NIAH) (Kamradt, 2023), with sequence lengths reaching

¹<https://huggingface.co/gradientai/Llama-3-8B-Instruct-262k>

Table 11. End-to-end metrics on Llama2 (7B).

Model	Attention	WikiText (Ppl.) ↓	Lambda (Acc.) ↑	MMLU (Acc.) ↑
Llama2	Full-Precision	5.823	0.886	0.439
	HadmdAttn	6.771	0.860	0.360
	SmoothAttn	6.717	0.867	0.392
	SageAttention	5.824	0.887	0.439
	SageAttn2-4b	5.912	0.881	0.428
	SageAttn2-8b	5.828	0.886	0.438

Table 12. End-to-end metrics on CogvideoX (2B).

Model	Attention	CLIPSIM ↑	CLIP-T ↑	VQA-a ↑	VQA-t ↑	FScore ↑
CogvideoX (2B)	Full-Precision	0.1836	0.9975	77.605	75.360	3.006
	HadmdAttn	0.1742	0.9877	29.780	23.985	0.499
	SmoothAttn	0.1741	0.9870	41.703	47.043	0.624
	SageAttention	0.1833	0.9976	76.997	71.360	2.988
	SageAttn2-4b	0.1821	0.9973	77.368	74.906	2.603
	SageAttn2-8b	0.1829	0.9977	76.532	74.281	2.941

Table 13. End-to-end metrics on an image classification model.

Model	Attention	ImageNet (Acc.) ↑	Sketch (Acc.) ↑	ImageNet-r (Acc.) ↑
TIMM	Full-Precision	84.79%	45.32%	59.55%
	HadmdAttn	84.50%	44.89%	58.80%
	SmoothAttn	84.40%	44.68%	58.73%
	SageAttention	84.74%	45.38%	59.95%
	SageAttn2-4b	86.67%	45.24%	59.29%
	SageAttn2-8b	84.79%	45.39%	59.57%

Table 14. Comparison with FlashAttention3(fp8) on Llama-3-262k (8B) on InfiniBench (Zhang et al., 2024) (H100 GPU).

Attention	Eng.Sum	Eng.QA	Eng.MC	Code.Debug	Math.Find	Retr.PassKey	Retr.Num	Retr.KV	Avg.
Full-Precision	18.03	12.5	64.19	24.37	18.29	100.0	100.0	7.0	43.05
FlashAttn3-fp8	19.03	11.73	55.90	22.59	22.57	100.0	100.0	0.4	41.53
SageAttention2	18.17	12.46	64.19	25.63	17.43	100.0	100.0	6.6	43.06

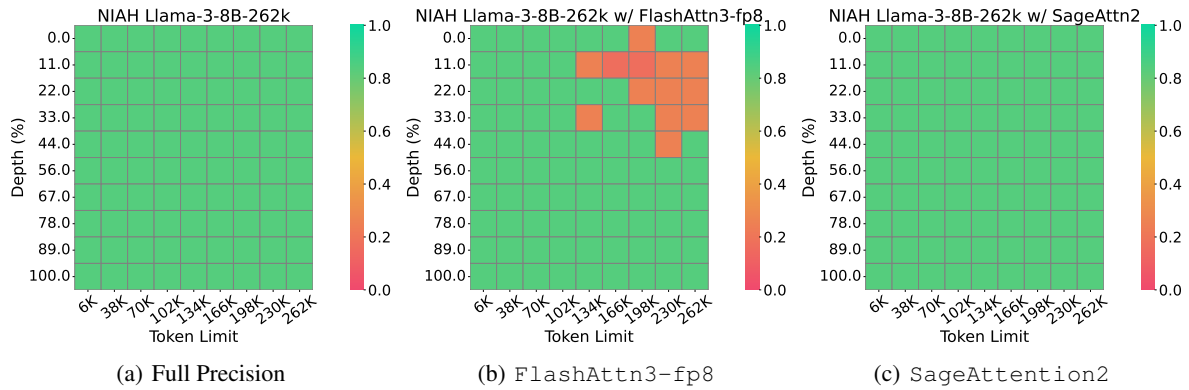


Figure 18. Needle In A Haystack results on Llama-3-262k (8B).

up to 262k tokens on an H100 GPU. Results are shown in Table 14 and Fig 18. SageAttention2 maintains model performance even under super-long context, while FlashAttention3(fp8) suffers from end-to-end accuracy degradation.

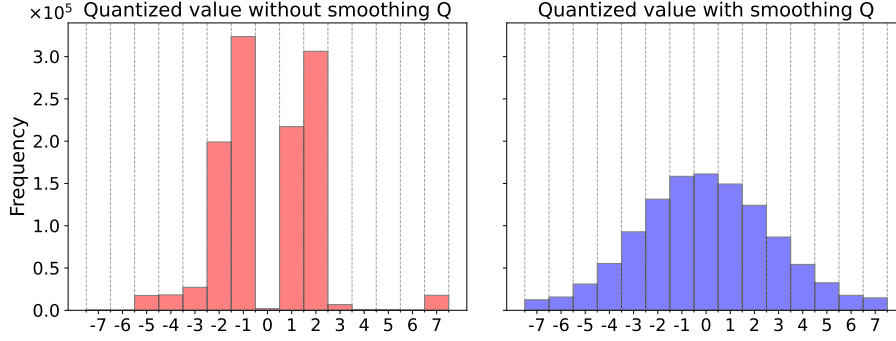

 Figure 19. An example of quantized value distribution of Q before and after smoothing Q .

 Table 15. **Worst accuracy** across all layers of CogvideoX using different quantization granularities.

Method	Cos Sim \uparrow	Relative L1 \downarrow	RMSE \downarrow
Per-token	96.76%	0.1916	0.0775
Per-thread	96.72%	0.1932	0.0776
Per-block	90.68%	0.3615	0.1490
Per-tensor	85.85%	0.4687	0.2261

 Table 16. **Worst accuracy** using different data types of (\tilde{P}, V) across all layers of a CogvideoX model, where (Q, K) are smoothed.

Q, K	\tilde{P}, V	Cos Sim \uparrow	Relative L1 \downarrow	RMSE \downarrow
INT4	INT8	19.52%	0.9579	1.4483
	E5M2	94.94%	0.2327	0.2361
	E4M3	96.70%	0.1956	0.0779
	FP16	96.76%	0.1916	0.0775

 Table 17. **Worst accuracy** across all layers of CogvideoX using different smooth methods.

Method	CosSim \uparrow	Relative L1 \downarrow	RMSE \downarrow
None	4.83%	0.9979	0.7784
HadmdAttn	4.85%	0.9978	0.7785
SmoothAttn	64.49%	0.9262	0.7204
Smooth K (Ours)	90.86%	0.3565	0.1464
Smooth Q (Ours)	93.10%	0.2989	0.2195
SageAttn2-4b	96.71%	0.1956	0.0779

Table 18. Overhead of per-thread quantization, smoothing Q, and two-level accumulation techniques measured on L20 GPU.

Method	TOPS
Attention (INT4 + FP8)	284
+ Per-thread quantization	283
+ Two-level accumulation	283
+ Smoothing Q	273